Robust State Space Embedded Control of a 3D Printed Permanent Magnet Synchronous Motor

Sergio Velarde-Gomez, Eduardo Giraldo

***Abstract*—This paper focuses on the design of a novel robust state-space embedded adaptive controller applied over a 3D printed permanent magnet synchronous motor (PMSM) with a radial Halbach array structure. The controller design is based on an extended state space representation with exogenous inputs. The control technique employed is the eigenstructure assignment, which positions the poles using the eigenvalues and eigenvectors. The design of the eigenstructure controller using an adaptive model with exogenous inputs results in a novel adaptive robust control strategy robust control. The performance of the proposed controller is evaluated over a simulated permanent magnet synchronous motor and a 3D-printed PMSM prototype.**

***Index Terms*—Robust, state space, adaptive control, identification, speed control.**

I. Introduction

OVER the years, research on the design of PMSMs as in [1] has shown that compared to induction motor (IM) or wound rotor synchronous motors (SM), PMSMs have a higher torque-to-inertia ratio and a higher power density. These motor characteristics depend on the type of magnets used and their location on the rotor. PMSMs can be classified into two broad categories, those that can be found with their permanent magnets mounted on the rotor surface and those that have their magnets buried inside the rotor.

The PMSM control can be designed based on the identification of multivariable systems, as proposed in [2], [3]. On the other hand, several approaches for optimal control can also be considered by using approximation or linearization but requiring a model, as described in [4], [5], [6].

In this work, a design of a novel extended state space embedded adaptive controller over a permanent magnet synchronous motor. The controller design is based on an extended state space representation with exogenous inputs. The control technique employed is the eigenstructure assignment, which positions the poles using the eigenvalues and eigenvectors. The design of the eigenstructure controller by using an adaptive model with exogenous inputs results in a novel adaptive robust control strategy. The performance of the proposed controller is evaluated over a simulated permanent magnet synchronous motor and a real 3D printed PMSM prototype with Halbach array structure. The prototype is coupled with a PMSM motor for load disturbances. This paper is organized as follows: in section II, the theoretical framework of the PMSM, and the control technique are presented. In section III are presented the results of the simulation and the PMSM prototype. Finally, the conclusions and future works are presented in section IV.

Manuscript received April 18, 2023; revised December 5, 2023.

Sergio Velarde-Gomez is a doctoral student in Electrical Engineering at Universidad Tecnológica de Pereira, Pereira, Colombia. Research Group in Automatic Control. E-mail: svelarde@utp.edu.co.

Eduardo Giraldo is a Full Professor at the Department of Electrical Engineering, Universidad Tecnológica de Pereira, Pereira, Colombia. Research group in Automatic Control. E-mail: egiraldos@utp.edu.co.

II. Theoretical Framework

A. PMSM Modeling

The PMSM modeling is detailed in [7], where (1) shows voltages across the stator windings

$$\begin{bmatrix} V_a \\ V_b \\ V_c \end{bmatrix} = \begin{bmatrix} R_s & 0 & 0 \\ 0 & R_s & 0 \\ 0 & 0 & R_s \end{bmatrix} \begin{bmatrix} i_a \\ i_b \\ i_c \end{bmatrix} + \begin{bmatrix} \frac{d\psi_a}{d_t} \\ \frac{d\psi_b}{d_t} \\ \frac{d\psi_c}{d_t} \end{bmatrix} \tag{1}$$

where:

- $\boldsymbol{V}_a$,$\boldsymbol{V}_b$ and $\boldsymbol{V}_c$ are the individual phase voltages across the stator windings.
- $\boldsymbol{R}_s$ is the equivalent resistance of each stator winding.
- $\boldsymbol{I}_a$,$\boldsymbol{I}_b$ and $\boldsymbol{I}_c$ are the currents flowing in the stator windings.
- $\frac{d\psi_a}{d_t}$, $\frac{d\psi_b}{d_t}$ and $\frac{d\psi_c}{d_t}$ are the rates of change for the magnetic flux in each stator winding.

Equation (2) shows the total flux formed by the permanent magnets and each of the three windings.

$$\begin{bmatrix} \psi_a \\ \psi_b \\ \psi_c \end{bmatrix} = \begin{bmatrix} L_{aa} & L_{ab} & L_{ac} \\ L_{ba} & L_{bb} & L_{bc} \\ L_{ca} & L_{cb} & L_{cc} \end{bmatrix} \begin{bmatrix} i_a \\ i_b \\ i_c \end{bmatrix} + \begin{bmatrix} \psi_{am} \\ \psi_{bm} \\ \psi_{cm} \end{bmatrix} \tag{2}$$

where:

- ψ_a, ψ_b and ψ_c are the total fluxes linking each stator winding.
- $\boldsymbol{L}_{aa}$, $\boldsymbol{L}_{bb}$ and $\boldsymbol{L}_{cc}$ are the self-inductances of the stator windings.
- $\boldsymbol{L}_{ab}$, $\boldsymbol{L}_{ac}$, $\boldsymbol{L}_{ba}$ and so on, are the mutual inductances of the stator windings.
- ψ_{am}, ψ_{bm} and ψ_{cm} are the permanent magnet fluxes linking the stator windings.

The inductances in the stator windings are functions of the rotor electrical angle and defined by

$$\begin{aligned}
\theta_e &= N\theta_r + \text{rotor offset} \\
L_{aa} &= L_s + L_m \cos(2\theta_e) \\
L_{bb} &= L_s + L_m \cos\left(2(\theta_e - \frac{2\pi}{3})\right) \\
L_{cc} &= L_s + L_m \cos\left(2(\theta_e + \frac{2\pi}{3})\right) \\
L_{ab} &= L_{ba} = -M_s - L_m \cos\left(2(\theta_e + \frac{\pi}{6})\right) \\
L_{bc} &= L_{cb} = -M_s - L_m \cos\left(2(\theta_e + \frac{\pi}{6} - \frac{2\pi}{3})\right) \\
L_{ca} &= L_{ac} = -M_s - L_m \cos\left(2(\theta_e + \frac{\pi}{6} + \frac{2\pi}{3})\right)
\end{aligned}$$

where:

- θ_r is the rotor mechanical angle.
- θ_e is the rotor electrical angle.
- rotor offset is θ if you define the rotor electrical angle with respect to the $d-axis$, or$-\pi/2$ if you define the rotor electrical angle with respect to the $q-axis$
- $\boldsymbol{L}_s$ is the stator self-inductance per phase. This value is the average self-inductance of each of the stator windings.
- $\boldsymbol{L}_m$ is the stator inductance fluctuation. This value is the amount the self-inductance and mutual inductance fluctuate with the changing of the rotor angle.
- $\boldsymbol{M}_s$ is the stator mutual inductance. This value is the average mutual inductance between the stator windings.

Equation (3) shows the linked motor flux, considering the permanent magnet flux linking winding $\boldsymbol{a}$ is a maximum when $\theta_e = 0^o$ and zero when $\theta_e = 90^o$.

$$\begin{bmatrix}\psi_{am}\\ \psi_{bm}\\ \psi_{cm}\end{bmatrix} = \begin{bmatrix}\psi_m \cos\theta_e\\ \psi_m \cos(\theta_e - \frac{2\pi}{3})\\ \psi_m \cos(\theta_e + \frac{2\pi}{3})\end{bmatrix} \tag{3}$$

where ψ_m is the permanent magnet flux linkage.

Applying Park's transformation to the electrical equations described in the previous subsection, we obtain an expression for torque that is independent of rotor angle.

Equation (4) defines the Park´s transformation

$$P = \frac{2}{3}\begin{bmatrix}\cos\theta_e & \cos(\theta_e - \frac{2\pi}{3}) & \cos(\theta_e + \frac{2\pi}{3})\\ -\sin\theta_e & -\sin(\theta_e - \frac{2\pi}{3}) & -\sin(\theta_e + \frac{2\pi}{3})\\ 0.5 & 0.5 & 0.5\end{bmatrix} \tag{4}$$

where θ_e is the electrical angle defined as $\boldsymbol{N}\theta_r$. $\boldsymbol{N}$ is the number of pole pairs.

Using Park's transformation on the stator winding voltages (5) and currents (6) transforms them to the $\boldsymbol{dq0}$ frame, which is independent of the rotor angle:

$$\begin{bmatrix}v_d\\ v_q\\ v_0\end{bmatrix} = P\begin{bmatrix}v_a\\ v_b\\ v_c\end{bmatrix} \tag{5}$$

$$\begin{bmatrix}i_d\\ i_q\\ i_0\end{bmatrix} = P\begin{bmatrix}i_a\\ i_b\\ i_c\end{bmatrix} \tag{6}$$

Applying Park's transformation to the first two electrical equations produces these equations that define the block behavior:

$$\begin{aligned} v_d &= R_s i_d + L_d\tfrac{\mathrm{d}i_d}{d_t} - N\omega i_q L_q\\ v_q &= R_s i_q + L_q\tfrac{\mathrm{d}i_q}{d_t} + N\omega(i_d L_d + \psi_m)\\ v_0 &= R_s i_0 + L_0\tfrac{\mathrm{d}i_0}{d_t}\\ T &= \tfrac{3}{2}N(i_q(i_d L_d + \psi_m) - i_d i_q L_q)\end{aligned}$$

where:

- $L_d = L_s + M_s + 3/2\ L_m$. L_d is the stator $d-axis$ inductance.
- $L_q = L_s + M_s - 3/2\ L_m$. L_q is the stator $q-axis$ inductance.
- $L_0 = L_s - 2M_s$. L_0 is the stator zero-sequence inductance.
- ω is the rotor mechanical rotational speed.
- $\boldsymbol{N}$ is the number of rotor permanent magnet pole pairs.
- $\boldsymbol{T}$ is the rotor torque.

B. PMSM construction

1) Surface mounted PMSM: There are two variations in the surface mounted PMSM:

- The first variation in which the permanent magnets project from the surface of the rotor and which is called projecting type.
- In the second variation the magnets are embedded in the rotor itself generating a smooth surface, this variation is called inset type.

a) Projecting type: Permanent magnet synchronous motors with magnets mounted on the rotor surface are generally the cheapest and simplest in the industry. Their construction method is usually straightforward. Generally, their magnets are mounted on the rotor surface and glued with epoxy-type glue. Compared to other PMSM constructions, such as rotors with magnets inside the rotor, this assembly makes them unsuitable for high-speed applications. These motors have an almost uniform air gap because the relative permeability of the magnet is approximately equal to that of the air, generating that their inductances in the direct axis and the quadrature axis are equal. The projecting surface mounted PMSM. See Fig. 1 have only torque derived from the magnet flux, and thus no reluctance torque. Because this type of motor has a small inductance, the surface-mounted magnets have a large air gap in the magnetic circuit. Additionally, this small inductance value results in a lower stator time constant. They are usually built with a smaller rotor diameter producing motors of lower inertia and good dynamic performance. More elaborate versions of these motors are suitable for high-performance tool drives and industrial robots.

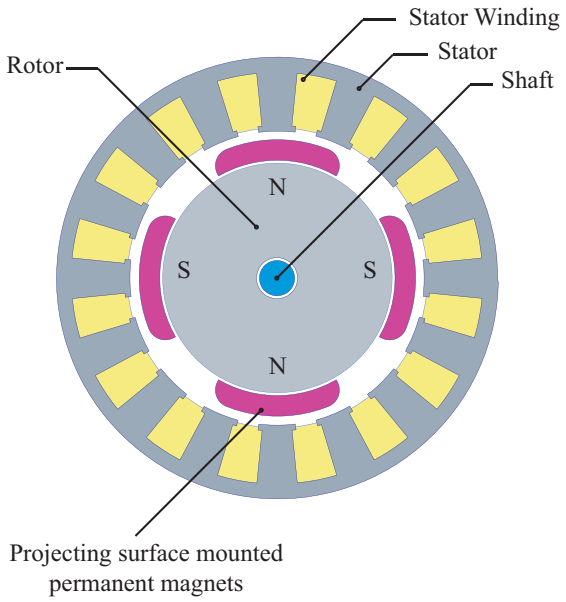

Fig. 1. Projecting surface mounted PMSM

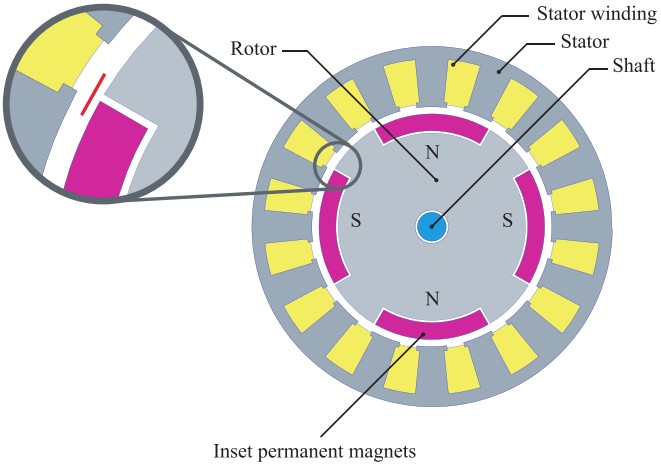

Fig. 2. Inset magnet PMSM

b) Inset type: Permanent magnet synchronous motors of the inset type are characterized by the fact that their magnets mounted on the rotor surface do not protrude from the rotor surface and are instead aligned with the rest of the rotor material, the red line highlights this alignment in Fig. 2

This location of the magnets allows the motor to be mechanically much more robust than compared to motors with Projecting surface-mounted PMSM. See Fig 1. in this magnet array mounted on the rotor, the quadrature inductance is higher than that of the direct shaft since the magnet is equivalent to an air gap on the direct shaft. This location outside the rotor results in a significant reluctance torque that adds to the magnetic torque.

In general, the Inset - PMSM rotor is very similar to the commonly used surface-mounted permanent magnet rotor, its main difference being the iron teeth or rotor teeth housed between each adjacent permanent magnet gap. Finally, its main advantage is that it has a more significant flux path in the rotor core compared to the surface-mounted PMSM [8].

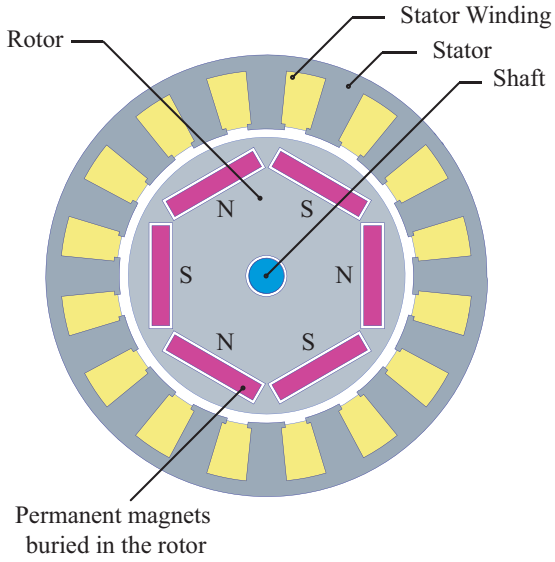

Fig. 3. Interior magnet PMSM

The second category of construction in which the magnets are embedded inside the rotor is described below, this type of construction is known as Interior PM (IPM).

2) Inner rotor PMSM: Inner rotor permanent magnet synchronous motors, see Fig. 4, are usually found more quickly in the market. They have advantages over outer rotor motors, among which is greater ease of cooling because the stator is attached directly to the outside of the motor, which allows more excellent heat dissipation, while an outer rotor PMSM usually needs its cooling system [9].

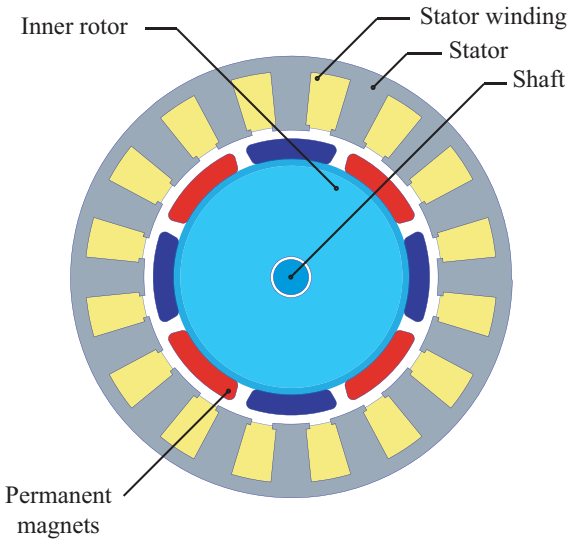

Fig. 4. Inner rotor PMSM

3) Outer rotor PMSM: A PMSM with an external rotor structure, see Fig 5, is intended to produce more torque. Due torque is directly proportional to the square value of the rotor diameter, which increases proportionately to the number of poles in the rotor [10].

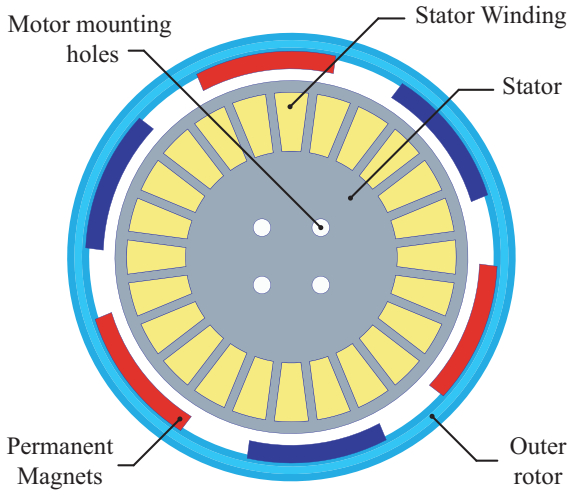

Fig. 5. Outer rotor PMSM

For this reason, PMSMs can increase their power density by increasing the number of poles of the motor and considering the controller's switching frequency. This feature creates a significant advantage for external rotor PMSMs. Since the rotor's radius is outside the stator's radius, it allows

a certain degree of freedom when it comes to increasing the number of poles on the motor. In the case of internal rotor motors, increasing the number of poles is complicated because the rotor is located inside the stator. If the number of poles of the PMSM is increased, the commutation frequency increases, generating a motor with a higher power density.

C. Extended state space adaptive control

An adaptive state space control strategy is proposed based on the identified parameters of the model by using a simplified approximation of the system. In this case, the projection algorithm, described in [11], is proposed as follows:

$$\theta[k] = \theta[k-1] + \frac{\phi[k-1]}{0.0001 + \phi^T[k-1]\phi[k-1]} \left(y[k] - \phi^T[k-1]\theta[k-1]\right) \tag{7}$$

being $\theta[k$ the vector of estimated parameters, and $\phi[k-1]$ the vector of past inputs and outputs, are defined as follows

$$\theta[k] = \begin{bmatrix} a_1 \\ b_0 \\ c_0 \end{bmatrix}, \phi[k-1] = \begin{bmatrix} -y[k-1] \\ u[k-1] \\ e[k-1] \end{bmatrix} \tag{8}$$

where $e[k]$ is the exogenous input related to estimation error and noise modeling, and where the second order extended state space model is defined as

$$x[k+1] = \begin{bmatrix} -a_1 & b_0 \\ 1 & 0 \end{bmatrix} x[k] + \begin{bmatrix} 0 \\ 1 \end{bmatrix} u[k] \tag{9}$$

with output equation

$$y[k] = \begin{bmatrix} -a_1 & b_0 \end{bmatrix} x[k] \tag{10}$$

being $x[k]$ the state space vector defined as

$$x[k] = \begin{bmatrix} y[k-1] \\ u[k-1] \end{bmatrix} \tag{11}$$

In order to perform a closed loop system, a control signal $u[k]$ is defined as

$$u[k] = -K_d x[k] + K_g r[k] \tag{12}$$

where $K_d = [K_1\, K_2]$ is the feedback matrix for the eigenvalues assignment, and is computed by assuming a closed loop dynamics $P(z) = z^2 - 0.67z$ as follows

$$K_d = \begin{bmatrix} 0 & 1 \end{bmatrix} \begin{bmatrix} 0 & b_0 \\ 1 & 0 \end{bmatrix}^{-1} \left(\begin{bmatrix} -a_1 & b_0 \\ 1 & 0 \end{bmatrix}^2 - 0.67 \begin{bmatrix} -a_1 & b_0 \\ 1 & 0 \end{bmatrix} \right) \tag{13}$$

$$= \begin{bmatrix} K_1 & K_2 \end{bmatrix} \tag{14}$$

and K_g the feed forward gain defined as

$$K_g = \frac{1}{\begin{bmatrix} -a_1 & b_0 \end{bmatrix} \begin{bmatrix} 1-a_1 & -b_0 \\ -1+K_1 & 1+K_2 \end{bmatrix}^{-1} \begin{bmatrix} 0 \\ 1 \end{bmatrix}} \tag{15}$$

III. Results

The proposed approach is evaluated by simulation and in real time by considered an identified PMSM plant and a real 3D Printed PMSM prototype with radial Halbach array structure which is coupled with another PMSM for load disturbances. The 3 The identified PMSM plant is defined as follows:

$$H(z) = \frac{22.59z - 19.52}{z^2 - 1.226z + 0.2759} \tag{16}$$

by considering a sample time of 250 ms.

The closed loop response for reference tracking is presented in Fig. 6.

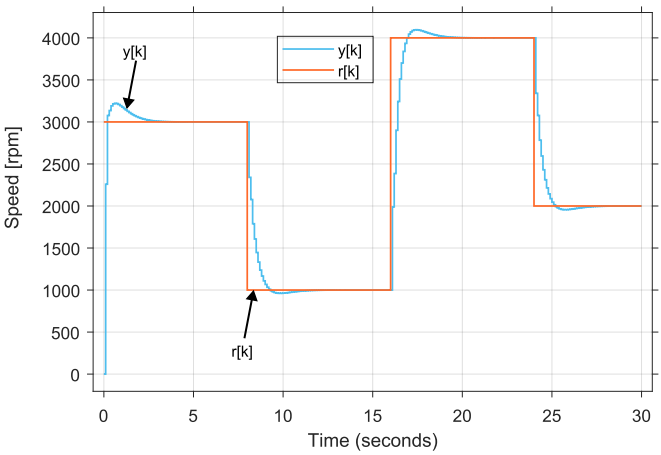

Fig. 6. Speed reference tracking

The closed loop control signal $u[k]$ for reference tracking presented in Fig. 6, is shown in Fig. 7.

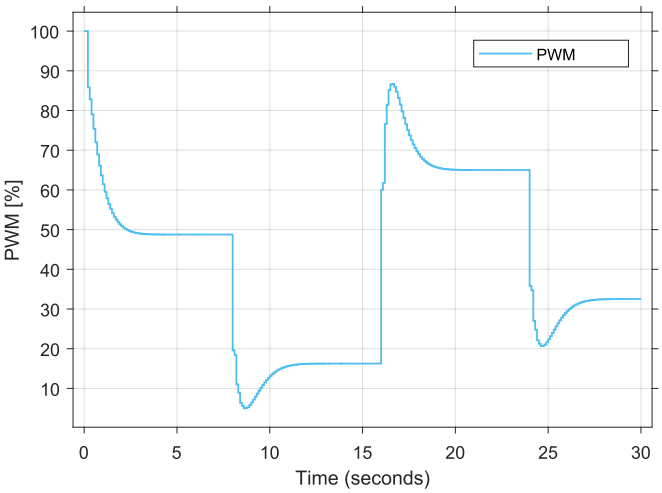

Fig. 7. PWM control signal for reference tracking

The parameter estimation for vector θ for the reference tracking presented in Fig. 6, is shown in Fig. 8.

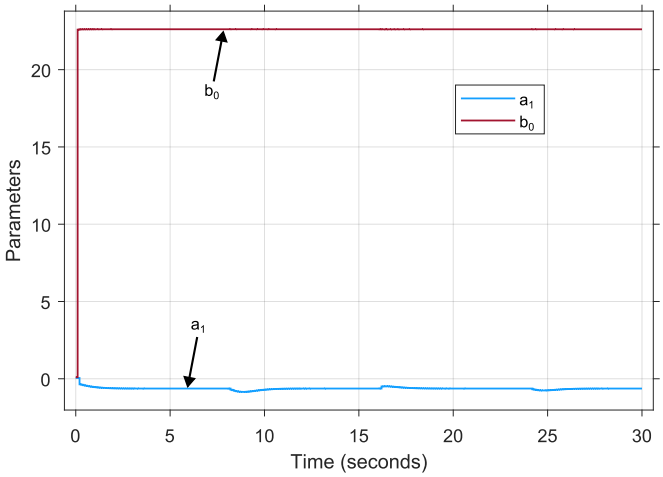

Fig. 8. Parameter estimation for reference tracking

The 3D printed PMSM prototype of 9 pair of poles is presented in Fig. 9. This PMSM is coupled to a quadrature encoder in order to obtain an indirect measurement of the speed in rpm.

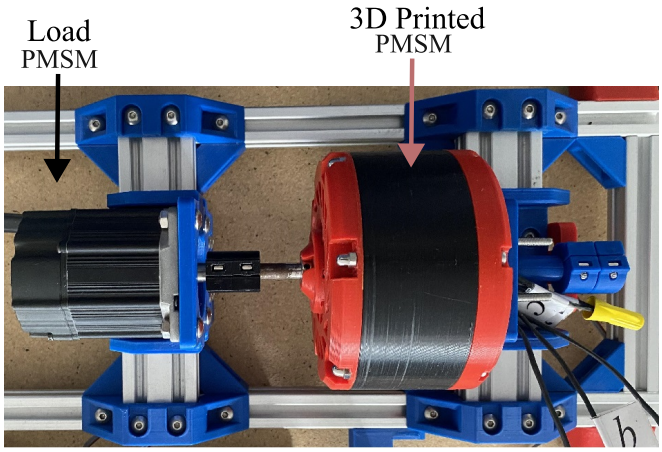

Fig. 9. PMSM Workbench for robust control

The controller algorithm is implemented in a C2000 Texas Instruments F28379D controller board by using a BoostXL-Drv8301 driver for the PMSM.

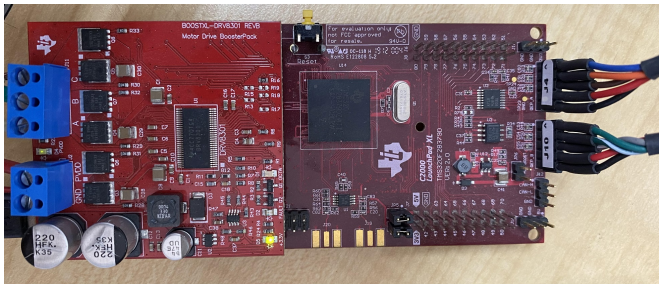

Fig. 10. C2000 F28379D board and Drv8301 driver

A soft start restriction is considered, where the max speed change is limited. In Fig. 11 is depicted the soft start for a reference tracking of 800 rpm. It is worth noting that after the soft start, the reference tracking is performed without restriction, as shown in Fig. 11 for a reference tracking of 600 rpm.

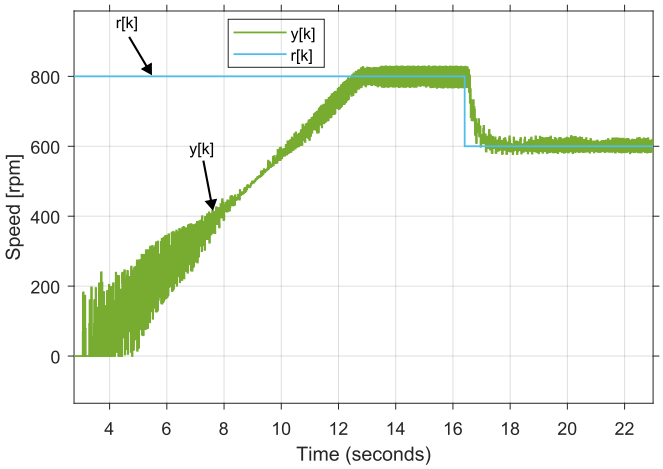

Fig. 11. Soft start for the real prototype

A detailed view of the reference tracking for a change between 800 rpm and 600 rpm is shown in Fig. 12. It is worth noting that this reference change is performed after the soft start.

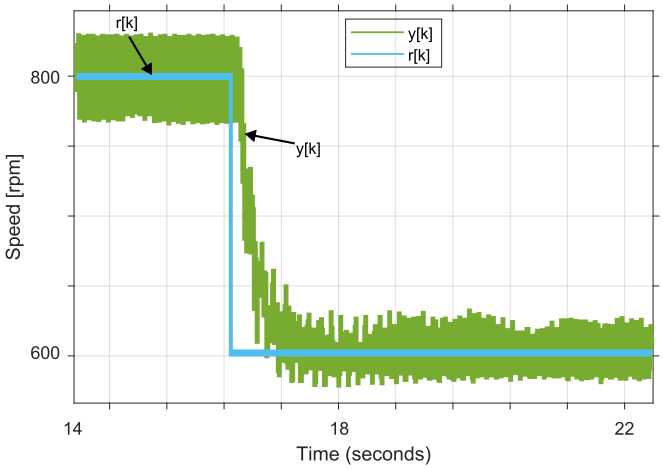

Fig. 12. Reference tracking for the real prototype after the soft start

In Fig. 13 is shown additional references tracking achieved after the soft start, by considering an initial reference of 700 rpm.

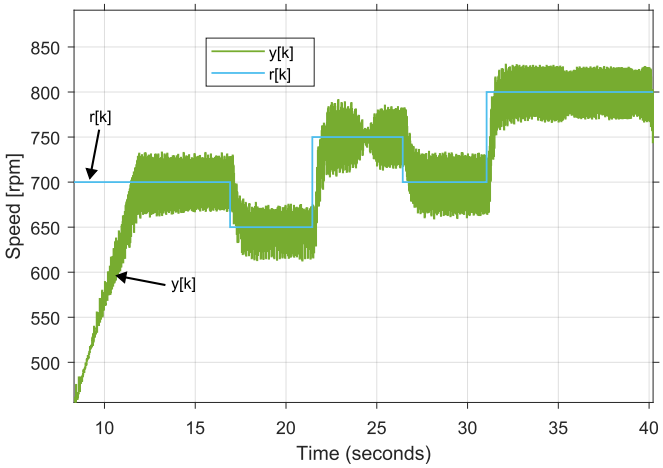

Fig. 13. Reference tracking after the soft start for the real prototype

In Fig. 14 is shown the reference tracking by considering

an initial reference of 500 rpm and increments of 100 rpm.

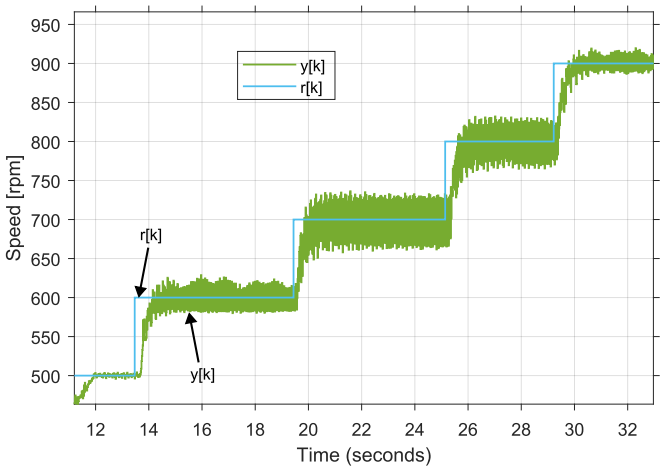

Fig. 14. Incremental reference tracking after the soft start for the real prototype

In Fig. 15 is shown a detailed view of a reference change from 500 to 600 rpm. It can be seen that the reference is tracked even in the presence of noise.

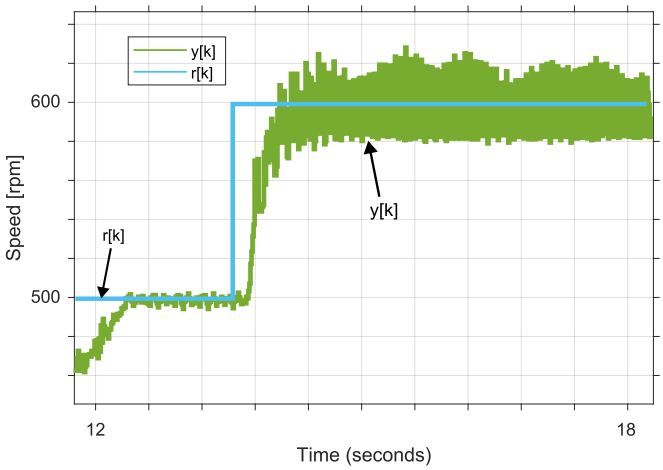

Fig. 15. Detailed view of an incremental reference tracking after the soft start for the real prototype

In Fig. 16 is shown the reference tracking by considering impulse disturbances around 500 rpm applied a time instants 14 seconds, 22 seconds and 28 seconds.

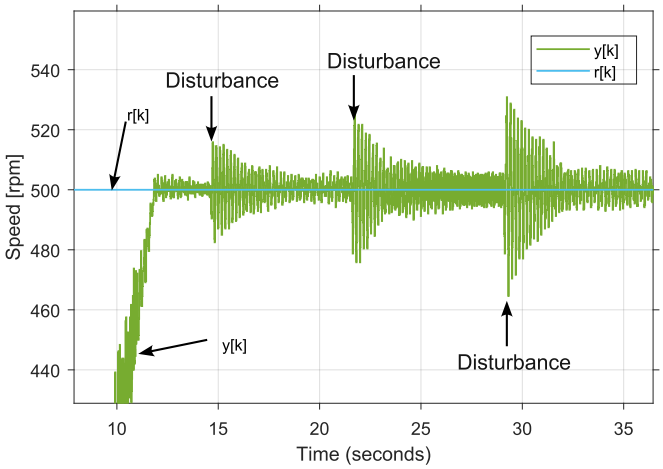

Fig. 16. Reference tracking under impulse disturbances for the real prototype around 500 rpm

In Fig. 17 is shown the reference tracking by considering one impulse disturbance around 500 rpm applied a time instant 14 seconds. It is worth noting that the system response tends to the reference. The settling time is held around 3 seconds even under presence of noise.

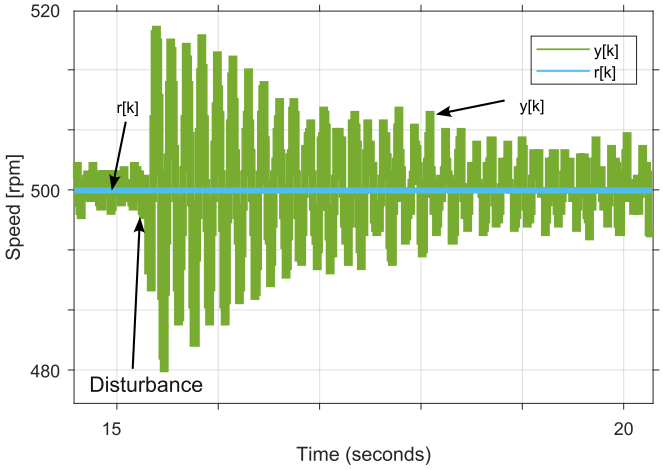

Fig. 17. Detailed reference tracking under one impulse disturbance for the real prototype around 500 rpm

In Fig. 18 is shown the reference tracking by considering impulse disturbances around 1000 rpm applied a time instants 16 seconds, 21 seconds and 27 seconds.

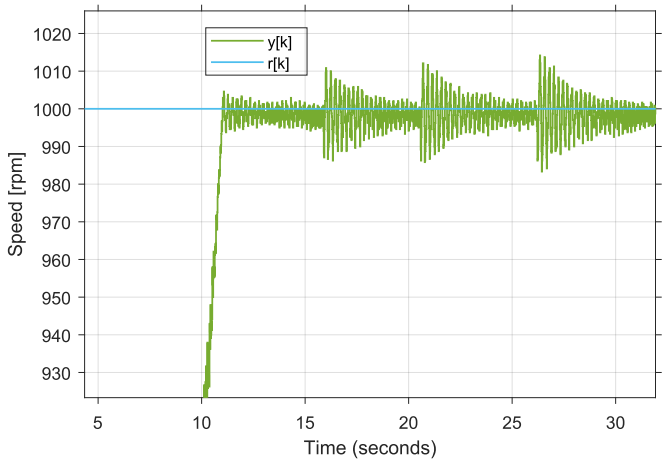

Fig. 18. Reference tracking under impulse disturbances for the real prototype

It is worth noting that the system response tends to the reference after each impulse response is applied. The settling time is held around 4 seconds even under presence of noise.

IV. Conclusions

In this work, an adaptive state space robust embedded control is designed for PMSM with a Halbach array constructed through 3D printing. A closed-loop speed control system is implemented over a real-time C2000 F28379D Texas Instruments system in order to developed a speed reference tracking. It can be concluded, that the proposed approach effectively tracks any speed variation based on the identified model. In addition, it can be seen that the proposed approach can be applied to any PMSM modification even under uncertainties related to the mechanical and electrical parts. It can be seen that the speed reference is successfully achieved even under load disturbances. As future work, it is expected to evaluate the characterization of the motor in terms of torque and speed. Additionally, it is expected to obtain different configurations and geometries using 3D printing.

References

[1] R. Krishnan and A. Beutler, "Performance and design of an axial field PM synchronous motor servo drive," in *Conference Record - IAS Annual Meeting (IEEE Industry Applications Society)*, 1985, pp. 634–640.

[2] F. Osorio-Arteaga, J. J. Marulanda-Durango, and E. Giraldo, "Multivariable adaptive control of time-varying systems," *IAENG International Journal of Computer Science*, vol. 47, no. 4, pp. 605–612, 2020.

[3] J. Marulanda-Durango, A. Escobar-Mejia, and E. Giraldo, "Multivariable coupled control of a static var compensator to improve the power factor of a steel plant with an electric arc furnace load," *Engineering Letters*, vol. 29, no. 2, pp. 365–372, 2021.

[4] P. Hamedani and A. Shoulaie, "Indirect field oriented control of linear induction motors considering the end effects supplied from a cascaded h-bridge inverter with multiband hystersis modulation," in *4th Annual International Power Electronics, Drive Systems and Technologies Conference*, 2013, pp. 13–19.

[5] K. Wang, Y. Li, Q. Ge, and L. Shi, "Indirect field oriented control of linear induction motor based on optimized slip frequency for traction application," in *2016 18th European Conference on Power Electronics and Applications (EPE'16 ECCE Europe)*, 2016, pp. 1–10.

[6] S. Sanchez-Acevedo, D. Giraldo-Buitrago, and E. Giraldo, "Control lineal indirecto de campo del motor de induccion," *Scientia et Technica*, vol. 15, no. 40, pp. 279–284, 2008.

[7] *Power System Stability And Control*, ser. EPRI power system engineering series. McGraw-Hill, 1994. [Online]. Available: https://books.google.com.co/books?id=v3RxH_GkwmsC

[8] T. Nur and M. Mulyadi, "Improve cogging torque method in inset-permanent magnet synchronous machine," *Proceedings of 4th IEEE International Conference on Applied System Innovation 2018, ICASI 2018*, pp. 1211–1213, 2018.

[9] H. M. Taha and I. Alnaab, "Designs of PMSMs with Inner and Outer Rotors for Electric Bicycle Applications," *Kurdistan Journal of Applied Research*, vol. 4, no. 1, pp. 20–25, 2019.

[10] C.-H. Zhao, H. Qin, and Y.-G. Yan, "Analysis of the pole numbers on flux and power density of ipm synchronous machine," vol. 2, 2005, Conference paper, p. 1402 – 1407, cited by: 8; Conference name: Sixth International Conference on Power Electronics and Drive Systems, PEDS 2005; Conference date: 28 November 2005 through 1 December 2005; Conference code: 69272. [Online]. Available: https://www.scopus.com/inward/record.uri?eid=2-s2.0-33847278983&partnerID=40&md5=5e8c5b99db23f8cc411e9f82729fdfa6

[11] G. C. Goodwin and K. S. Sin, *Adaptive Filtering, Prediction and Control*. Englewood-Cliffs: Dover Publications Inc., 2009.